Supporting information for:

Photoconductivity Multiplication in Semiconducting Few-Layer $MoTe_2$

Wenhao Zheng [†], *Mischa Bonn*[†], *Hai I. Wang*[†*]

† Max Planck Institute for Polymer Research, Ackermannweg 10, 55128 Mainz, Germany;

*Email: wanghai@mpip-mainz.mpg.de

Content

1. Estimating band gap energy E_g using Tauc plots.

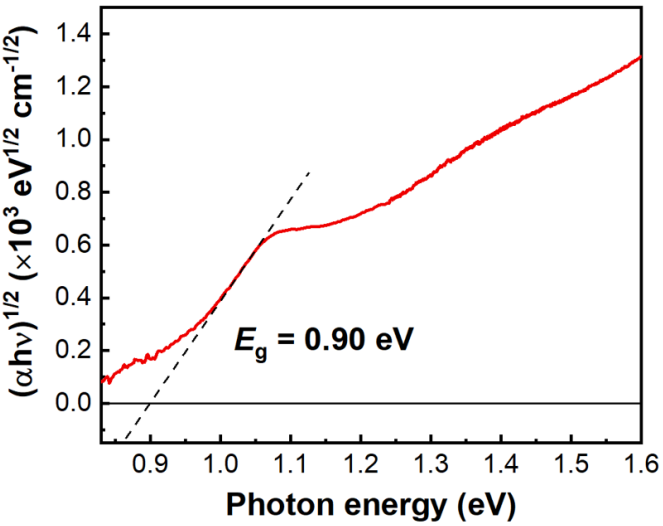

Figure S1. Optical band gap estimation for few-layer 2H-$MoTe_2$ using the Tauc plot method, based on UV-vis absorption spectrum.

Based on previous theoretical calculations[1], $MoTe_2$ with more than three layers (e.g. in our case) shows an indirect bandgap type, which involves the *K*-*Λ* transition. In order to quantify the bandgap energy, we apply Tauc plot analysis, as shown in **Figure S1**. Based on the fitting, we infer the bandgap to be ~ 0.9 eV. Note that this value is in line with previous experimental values (0.85 eV based on 17 nm thick $MoTe_2$ film).[2]

2. The origin for the fast decay in carrier dynamics for few-layer $MoTe_2$;

As shown in **Figure 2(b)**, the decay dynamics in the THz photoconductivity is directly related to decreasing of charge carrier density in the materials. Based on a previous study by Chen *et al*., the intrinsic band to band recombination process in exploited $MoTe_2$ can go up tonanosecond, which implies that the ultrafast sub-10 ps carrier density decay is related to trapping process to the defects present in the sample.[3] Such claim is supported by the same study by Chen *et al*.[3] and further by Kim *et al*.[2], in which a similar fast carrier decay is shown in MBE-grown $MoTe_2$ with high density of boundary/edge defect states.

To further discuss the nature of the trapping process and how the defects affect the carrier dynamics, e.g. by trapping of the charge carrier species (i.e. electron or/and hole), or trap-assisted recombination process (known also as Shockley–Read–Hall (SRH) recombination), we compared our THz conductivity dynamics to that of transient absorption (TA) data from Kim *et al.* (Figure 3a in Ref 2). It is worth to emphasizing the difference in tools and thus physical observables between THz spectroscopy and TA: while THz spectroscopy probes the photoconductivity (i.e. the product of carrier density and mobility), TA studies the population (i.e. only carrier density) dynamics of given excited states. In spite of all these differences, the TA and THz dynamics look similar: following a fast decay, we observe a long-lived dynamics with ~20% signal weight. This long-lived dynamics rules out the trap-assisted recombination as the main recombination channel and favors the scenario of electron or hole trapping process. If this is not the case, one would expect both TA and THz conductivity decay to ~0% following the trap-assisted recombination.

3. Photoconductivity dynamics of 2H-$MoTe_2$ with 3.1 eV photo-excitation energy.

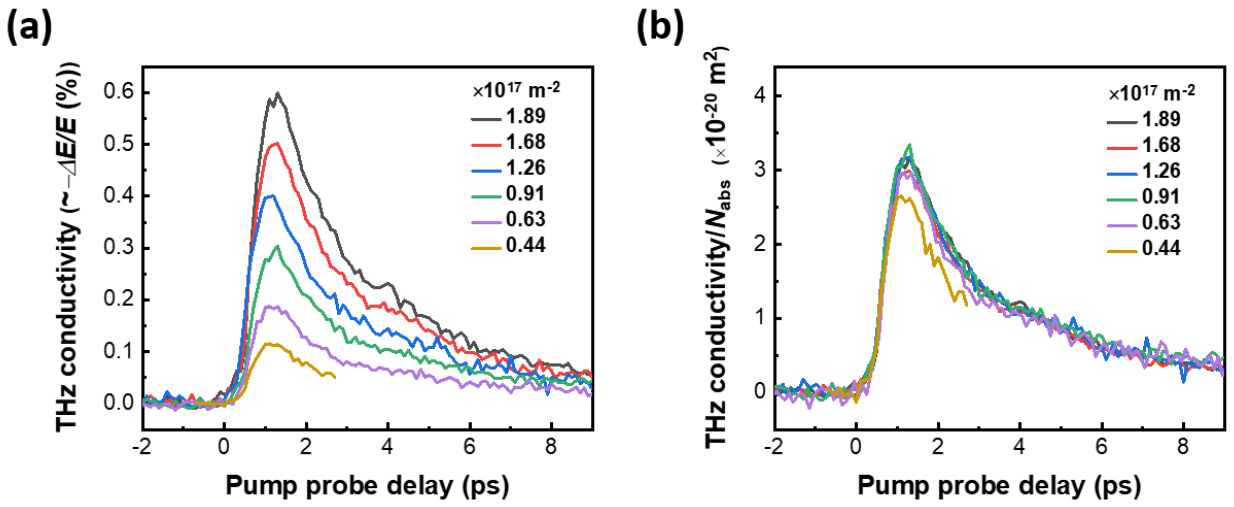

Figure S2 (a) The fluence-dependent THz conductivities as a function of pump–probe delay for 3.10 eV photon excitation; (b) The THz conductivities normalized to the absorbed photon density based on the data in (a).

4. THz time-domain spectroscopy.

For studying the electrical transport properties of photogenerated carriers, instead of tracking only the photo-induced THz field changes (ΔE) at the peak of the terahertz field transient, here we record the entire transmitted THz waveform in time domain with and without photoexcitation (E_{pump}(t) and E_0(t)), and analyze the data in frequency domain using Fourier transformations. The complex photoconductivity at THz frequencies can then readily be obtained using the thin-film approximation:

$$\Delta\sigma(\omega) = -\frac{n+1}{Z_0 \cdot l} \cdot \frac{(E_{pump}(\omega) - E_0(\omega))}{E_0(\omega)},$$

where Z_0 = 377 Ω is the impedance of free space, l is the thickness of the sample, and n = 1.77 is the refractive index of the sapphire substrate.

As discussed in the main text, the obtained frequency-resolved THz conductivities have been fitted further by the Drude and Drude-Smith model (see also more details in the next sections in **SI**). In principle, the applicability of Drude and Drude-Smith fittings requires that the time-domain measurements are conducted in a "quasi steady-state", in which e.g. the density of charge carriers is constant for the duration of the terahertz pulse. If the decay is faster, one can ensure that different parts of the terahertz pulse 'see' the same charge density by conducting the THz spectroscopy in such a way that the sampling laser pulse (the one used for electro-optic detection) and the pump pulse (the one used for the excitation) are at a fixed delay (by moving them simultaneously together). As there are three beams involving in the setup (THz generation, optical excitation and THz sampling pulses), this way of detection is equivalent to delaying only the THz generation beam, so that the time-delay between the pump and sampling pulses is fixed at a given optical pump – THz probe delay. This ensures that every time point within the THz probe transient corresponds to the same optical pump – THz probe delay, and relaxes the requirement of quasisteady-state to the ~40 femtosecond duration of the sampling pulse. The validity of this approach for conducting time-domain studies of the fast decay dynamics has been demonstrated previously.[4-5]

To further verify our discussion, we have conducted an additional THz time-domain (TDS) measurement at 2.0 ps after the 1.55 eV optical excitation. Following the discussion in the main

text, we applied both the Drude and Drude-Smith model to fit the data. Based on the fittings, to make a quantitative correlation, we have calculated and plotted the carrier densities obtained from the fittings on the right *Y*-axis and compared them to the OPTP data on the left *Y*-axis (see the data in **Figure S3a** and **b** inferred from the Drude and Drude-Smith fittings). The rescaled carrier densities and photoconductivities overlap well at these two time delays for TDS measurements. This seems to validate the method used and implies that the photoconductivity decay originates from the reduction of carrier density (e.g., by trapping as discussed later), not from the change of carrier mobility.

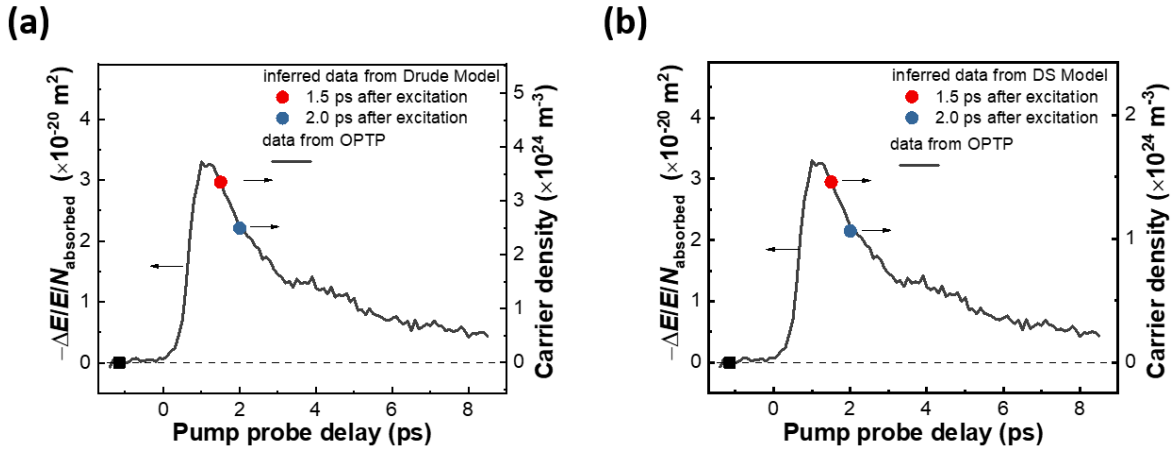

Figure S3. Comparison between THz photoconductivity dynamics (left *Y*-axis) and rescaled photogenerated carrier density inferred from the (a) Drude fitting and (b) Drude-Smith (DS) fitting.

5. Fitting the frequency-resolved data by Drude Model.

The substantial real conductivity and the close-zero imaginary contribution provide the fact that the generated carriers are largely present as free carriers (see **Figure 2e**). To describe the charge transport in $MoTe_2$, the standard Drude model is applied. In the Drude model, the electrons and holes are treated as an ideal classical gas, and the interactions with the lattice are assumed to take place through momentum randomizing scattering events, occurring with a mean scattering time. This model has been widely employed to other 2D materials.[6] The conductivity predicted by the Drude model provides a suitable description:

$$\sigma(\omega) = \frac{\omega_p^2 \varepsilon_0 \tau}{1 - i\omega\tau}, \text{ with } \omega_p^2 = \frac{e^2 N}{\varepsilon_0 m^*}$$

in which τ, ω_p, ε_0 and m^* are the scattering time, the plasma frequency, vacuum permittivity, and charge effective mass, respectively.

6. Comparison of the normalized frequency-resolved THz conductivity for excitations of 1.55 and 3.1 eV.

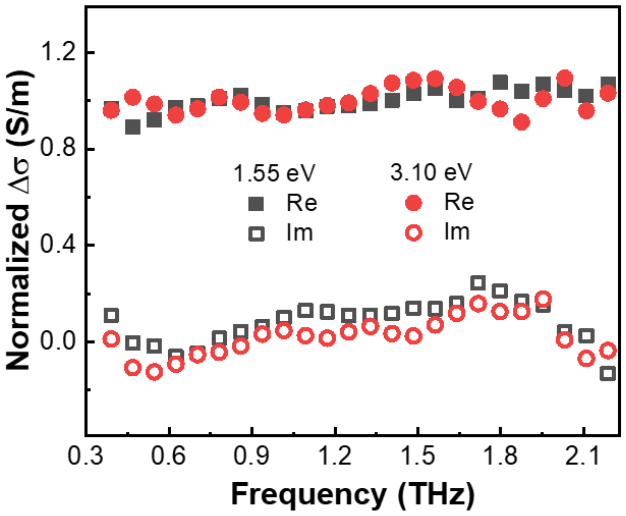

Figure S4. Normalized frequency-resolved THz conductivity for excitations of 1.55 and 3.1 eV.

7. Fitting the frequency-resolved data by Drude-Smith Model.

To shed light on the electrical transport properties in $MoTe_2$, a modified Drude model (so called "Drude-Smith model (DS model)") is also considered. The DS model is commonly employed to describe the charge carriers, which are subject to preferential backscatterings due to nanoscale disorder (e.g. defect or grain boundaries). Accordingly, the DS model can be expressed as:

$$\sigma(\omega) = \frac{\omega_p^2 \varepsilon_0 \tau}{1 - i\omega\tau}\left(1 + \frac{c}{1 - i\omega\tau}\right)$$

in which, τ, ω_p, ε_0 and m^* are the carrier momentum scattering time, the plasma frequency, vacuum permittivity and charge effective mass, respectively. Here the parameter *c* ranges between 0 and -1. By fitting the frequency-resolved data with the model (**Figure S5**), both the scattering time (~46 fs) and backscattering parameter (~ -0.5) are found to be nearly identical when comparing 3.1 and 1.55 eV excitations. The only noticeable change between the DS fitting comes from the inferred plasma frequency, with ω_p of 130 ± 4 and 180 ± 8 THz for the sample with excitations of 1.55- and 3.10 eV, respectively. Based on the expression $\omega_p^2 = \frac{e^2 N}{\varepsilon_0 m^*}$, the carrier densities *N* can be inferred to be 1.46×10^{24} ± 8.97×10^{22} and 2.83×10^{24} ± 2.50×10^{23} m^{-3}. This corresponds to the photogenerated carrier density ratio between 1.55 and 3.1 eV ($\frac{N_{3.10eV}}{N_{1.55eV}}$) ~1.92. This number is very close to the THz photoconductivity ratio generated by 1.55 and 3.1 eV, as discussed in the main text, which provides an additional support for CM effect in our sample.

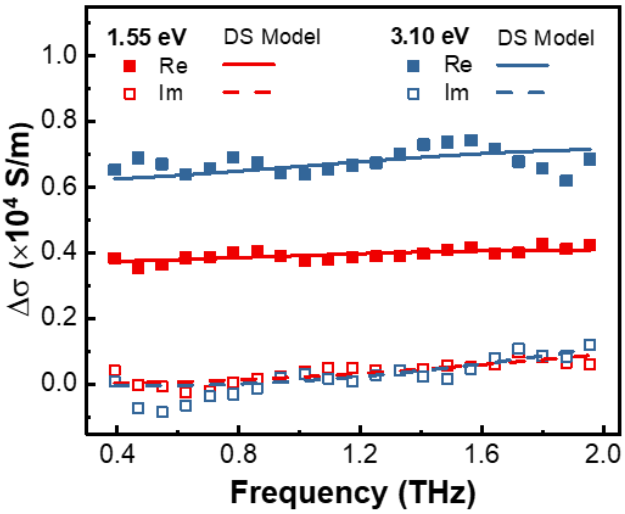

Figure S5. Complex, frequency-resolved THz conductivity measured at 1.5 ps after photon excitation with 1.55 and 3.10 eV excitations, respectively. The data are fitted by the Drude-Smith model described in the SI.

8. The normalized, pump energy-dependent OPTP dynamics.

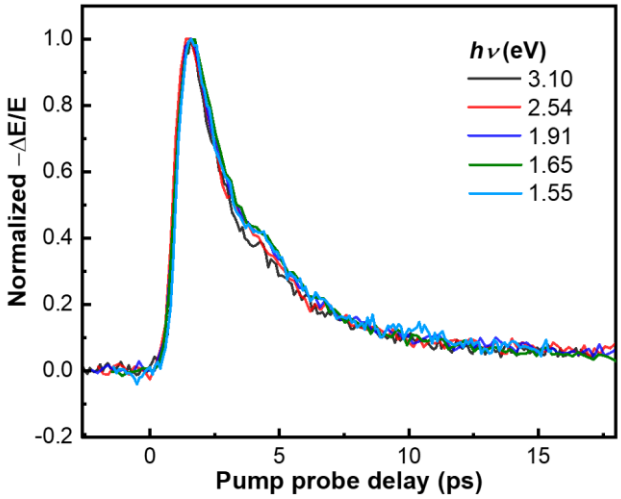

Figure S6. Normalized THz conductivity decay kinetics of few-layer 2H-$MoTe_2$ with different excitation photon energies

We find that the fast decay does not depend on the pump energies. This observation may be rationalized simply by the rate competition between the hot carrier cooling, CM and trapping process: the former two (sub-ps) are faster than that of the trapping (sub-10 ps), so that the trapping process takes place from the bandedge following cooling and CM processes.

9. To quantify the carrier multiplication efficiency.

Based on the model,[7] k_{II}/k_{cool} and the corresponding efficiency of CM (η_{CM}) can be expressed as:

$$QY = \sum_{j=1}^{m} j \frac{k_{cool}\prod_{i=1}^{j} k_{II}^{(i-1)}}{\prod_{i=1}^{j}(k_{cool}+k_{II}^{(i)})} \quad \text{where } k_{II}^{(0)} = 1\,,$$

$$\frac{k_{II}}{k_{cool}} = P\left(\frac{h\nu - h\nu_{th}}{h\nu_{th}}\right)^{s},$$

$$\eta_{CM} = \frac{P}{P+1}$$

Here, *m* denotes the number of additional photogenerated carriers reproduced by one hot carrier with sufficient excess energy above the bandgap. The parameter *P* describes the competition

between k_{II} and k_{cool}, and the exponential factor s is related to how the increasing excess energy affects k_{II}, whose typical value ranges from 2 to 5. Here, the exponent s is assumed to be 2 following the Keldysh formalism.

10. Discussion on CM onset energy difference between our and previous studies

The CM threshold energy is found to be ~2.5 eV (~2.8 times E_g) in our work, while ~1.7 eV in work from Kim *et al*.[2] The origin for such discrepancy remains unclear and requires further study. Here we provide some discussion based on previous theoretical studies. Thedifference in the CM onset energy may be due to the sample thickness (5 nm for our sample *vs.* 16.5 nm in Ref. 2) and thus electronic band structure in both samples. In the Ref. 2, a weak but clear indirect bandgap absorption (~0.85 eV) is observed, but it is clearly missing in our sample (see in **Figure 1c**). This observation could be rationalized by the thickness-dependent energetics of conduction band minimum (CBM) in $MoTe_2$. In the multilayer $MoTe_2$ with layer number n >4 (which is the case for our and Kim's samples), the band edge absorption corresponds to the Γ to Λ point optical transition. It has been shown previously the Λ point energy in the conduction band is thickness dependent and rises in the energetics towards vacuum with the decreasing the sample thickness.[1] The CBM at the bandedge transition plays an important role for CM. With a much higher CBM in the thinner $MoTe_2$ sample in our case (in comparison to that in Ref 2), there are less excess energies left for the CM. While this may be one of the possible sources for the different CM onset energies between our and Kim's report, further theoretical and experimental studies are required to solve this puzzle.

References

[1] Sun, Y.; Wang, D.; Shuai, Z., Indirect-to-Direct Band Gap Crossover in Few-Layer Transition Metal Dichalcogenides: A Theoretical Prediction. *J. Phys. Chem. C* **2016,** *120* (38), 21866–21870.

[2] Kim, J. H.; Bergren, M. R.; Park, J. C.; Adhikari, S.; Lorke, M.; Frauenheim, T.; Choe, D. H.; Kim, B.; Choi, H.; Gregorkiewicz, T.; Lee, Y. H., Carrier Multiplication in Van Der Waals Layered Transition Metal Dichalcogenides. *Nat. Commun.* **2019,** *10* (1), 5488.

[3] Chen, K.; Roy, A.; Rai, A.; Movva, H. C. P.; Meng, X.; He, F.; Banerjee, S. K.; Wang, Y., Accelerated Carrier Recombination by Grain Boundary/Edge Defects in MBE Grown Transition Metal Dichalcogenides. *APL Materials* **2018,** *6* (5), 056103.

[4] Ivanov, I.; Hu, Y.; Osella, S.; Beser, U.; Wang, H. I.; Beljonne, D.; Narita, A.; Mullen, K.; Turchinovich, D.; Bonn, M., Role of Edge Engineering in Photoconductivity of Graphene Nanoribbons. *J. Am. Chem. Soc.* **2017,** *139* (23), 7982–7988.

[5] Tries, A.; Osella, S.; Zhang, P.; Xu, F.; Ramanan, C.; Klaui, M.; Mai, Y.; Beljonne, D.; Wang, H. I., Experimental Observation of Strong Exciton Effects in Graphene Nanoribbons. *Nano Lett.* **2020,** *20* (5), 2993–3002.

[6] Lu, J.; Liu, H., A Critical Review on the Carrier Dynamics in 2D Layered Materials Investigated using THz Spectroscopy. *Opt. Commun.* **2018,** *406*, 24–35.

[7] Beard, M. C.; Midgett, A. G.; Hanna, M. C.; Luther, J. M.; Hughes, B. K.; Nozik, A. J., Comparing Multiple Exciton Generation in Quantum Dots to Impact Ionization in Bulk Semiconductors: Implications for Enhancement of Solar Energy Conversion. *Nano Lett.* **2010,** *10* (8), 3019–3027.